Journal of Power Sources 212 (2012) 13–21

Contents lists available at SciVerse ScienceDirect

Journal of Power Sources

journal homepage: www.elsevier.com/locate/jpowsour

Cross-linked zwitterionic polyelectrolytes based on sulfonated poly(ether sulfone) with high proton conductivity for direct methanol fuel cells

Lie Chen [a,1], Lina Sun [a], Rong Zeng [a,1], Shuqin Xiao [a], Yiwang Chen [a,b,*]

[a] Institute of Polymers, Department of Chemistry, Nanchang University, 999 Xuefu Avenue, Nanchang 330031, China
[b] Jiangxi Provincial Key Laboratory of New Energy Chemistry, Nanchang University, 999 Xuefu Avenue, Nanchang 330031, China

ARTICLE INFO

Article history:
Received 27 December 2011
Received in revised form
31 March 2012
Accepted 2 April 2012
Available online 13 April 2012

Keywords:
Polyelectrolytes
Poly(ether sulfone)
Zwitterion
Sol-gel

ABSTRACT

Hybrid cross-linked membranes of SPES/TEOS/TPABS for direct methanol fuel cells (DMFCs) are synthesized by sulfonated poly(ether sulfone) (SPES), tetraethoxysilane (TEOS) and a zwitterionic silica containing sulfonic acid and ammonium groups, 3-[[3-(triethoxysilyl)-propyl]amino]butane-1-sulfonic acid (TPABS) using a sol-gel process with the goal of obtaining high proton conductivity, low methanol permeability and good stability. Increasing the amount of inorganic zwitterionic TPABS produces membranes that become denser and more uniform. The increasingly SO_3-rich cross-linked networks consequently lead to higher proton conductivity and lower methanol permeability. It should be noted that the proton conductivity reaches as high as that of Nafion® 117, whereas the methanol permeability is greatly reduced by the formation of the cross-linked structures. Among these membranes, SPES/TEOS/TPABS-70 (70 wt % of TPABS to SPES in the membrane matrix), shows the best performance with a proton conductivity value of 7.24×10^{-2} S cm^{-1}, methanol permeability value of 2.46×10^{-7} cm^2 s^{-1}, ion-exchange capacity value of 1.37 mequiv g^{-1} and a comparable selectivity parameter of 2.63×10^5 S cm^{-3} s.

1. Introduction

Direct methanol fuel cells (DMFCs) are currently considered one of the most promising alternative power-delivery systems. The pivotal part in DMFCs is the polymer electrolyte membrane (PEM), which must possess several characteristics including high proton conductivity, low fuel and oxidant permeability, oxidative and hydrolytic stability, balanced water transport, good mechanical properties, and the capability to be assembled into a membrane electrode assembly (MEA) at low cost [1]. The non-hybrid membranes most often used in DMFCs are perfluorosulfonic acid (PFSA) membranes (e.g., Nafion®) [2,3]; however, perfluorosulfonic acid polymers are limited by their high methanol permeability and high cost [4]. For the development of better PEMs, fluorine-free materials with low cost, excellent thermal stability and other comparable properties to those of Nafion®, based on sulfonated aromatic polymers, irradiation graft polymers, and cross-linked polymers, have been successfully created [5].

Organic–inorganic hybrid membranes are one of the most promising materials for proton exchange membranes because they have both the attractive properties of an inorganic backbone (stable mechanical and thermal properties) and organo-functional groups which provide specific chemical activities and flexibility [6–8]. Among the various types of organic–inorganic composite membranes, Si-based nanocomposite materials are considered to be an effective way of improving the properties of proton conducting hybrid materials. The two methods of introducing silica into the polyelectrolytes are directly doping mesoporous silica into the polymer electrolyte or in-situ sol-gel template synthesis of mesoporous silica within the polymer matrix. However, directly doping usually results in system instability, due to poor molecular interactions, and may easily cause aggregation of the fillers in the polymer matrix.

During sol-gel processing, molecular precursors change into nano-sized particles [9,10]. The colloidal suspension, or sol, results in the formation of gel networks. Thus, in-situ sol-gel template synthesis of mesoporous silica in a polymer electrolyte is a feasible strategy for obtaining uniform and stable organic–inorganic hybrid membranes. Pereira et al. [11] reported the preparation of mesoporous silica-Nafion® hybrid membranes by in-situ sol-gel routes in the presence of templating agents like Pluronic. This approach has the advantage of growing ordered mesoporous silica in the Nafion®

* Corresponding author. Institute of Polymers, Department of Chemistry, Nanchang University, 999 Xuefu Avenue, Nanchang 330031, China. Tel.: +86 791 83969562; fax: +86 791 83969561.
E-mail address: ywchen@ncu.edu.cn (Y. Chen).
[1] Equal contribution.

0378-7753/$ – see front matter © 2012 Elsevier B.V. All rights reserved.
doi:10.1016/j.jpowsour.2012.04.008

polymer without disrupting the proton transport pathways. However, the amount of mesoporous silica introduced into the Nafion® matrix was relatively low. Tripathi et al.[12] reported the synthesis of an organic–inorganic hybrid zwitterionic silica precursor with ammonium and sulfonic acid functionality used to form cross-linked PEM by sol-gel synthesis in aqueous media, proving that in-situ sol-gel route is a flexible way of introducing a purely inorganic phase into a polymeric matrix; however, their conductivity levels have not yet fit for use in fuel cells.

In our previous work, we prepared sulfonated poly(ether sulfone ether ketone ketone)/sulfonated poly(ether sulfone) membranes though direct blending, and then characterised their properties as PEMs. Sulfonated poly(ether sulfone) shows potential as it possesses high proton conductivity, low methanol permeability and excellent mechanical strength. The high degree of sulfonation leads to high proton conductivity but can result in an unacceptable degree of swelling and unsatisfactory mechanical properties. Herein, we attempt to design and synthesize cross-linked nanocomposite membranes for DMFCs using 3-[[3-(triethoxysilyl)-propyl] amino] butane-1-sulfonic acid (TPABS) as an inorganic zwitterionic precursor by a sol-gel method. The inorganic nanoparticles would be stably fixed in a cross-linked structure formed by ammonium and sulfonic acid interactions. In addition, the high concentration of sulfonic acid groups and organic–inorganic cross-linked structures can further make a balance between proton conductivity and low fuel permeability. In this paper, the synthesis procedure for this new type of nanocomposite is reported, and the relationship between structures and properties of organic–inorganic nanocomposite is investigated.

2. Experimental

2.1. Materials

Poly (ether sulfone) (PES) was obtained from BASF (Ludwigahfen Germany), while (3-aminopropyl) triethoxysilane (APTES), tetraethoxysilane (TEOS), 1,4-butane sultone (BS) and Nafion®117 (perfluorinated membrane) were provided by Aladdin Chemistry Co. Ltd (Shanghai, China) and were used as received. Chlorosulfonic acid, concentrated sulphuric acid (H_2SO_4, 95–98%), dimethylacetamide (DMAc) and AR grade methanol were purchased commercially and used without further purification. Tetrahydrofuran (THF; Damao Chemicals, Tianjin, China) was distilled and kept dry with molecular sieves. Deionised water was used for all purposes.

2.2. Synthesis of SPES and TPABS

SPES was prepared according to the method described by Guan et al. [13]. The organic–inorganic precursor of the zwitterionomer, 3-[[3-(triethoxysilyl)-propyl]amino]butane-1-sulfonic acid (TPABS), was synthesized using APTES and 1,4-butane sultone (BS). APTES was dissolved in THF at ambient temperature under a nitrogen atmosphere; 1,4-butane sultone (BS) in THF was transferred into a dropper and then, slowly and gradually, added to the APTES solution which was kept at 50 °C. The resultant mixture was refluxed under slight stirring for 3 h under a nitrogen atmosphere, and the solvent was evaporated using a Rotary Evaporator producing a pale-yellow liquid (TPABS). ^{1}H NMR (500 MHz, $CDCl_3$, δ): 0.65 ($-SiCH_2CH_2-$), 1.2 and 3.7–3.8 ($-SiOC_2H_5-$), 1.9 ($-SiCH_2CH_2-$), 2.4 and 3.2 ($-NH_2^+CH_2CH_2CH_2CH_2SO_3^-$), 2.7–2.9 ($-CH_2NH_2^+CH_2-$).

2.3. Preparation of a SPES–TPABS composite membrane

The membranes were prepared in two steps using a solution-casting method. SPES (10 wt. %) was dissolved in DMAc to obtain a highly viscous solution under constant stirring; separately, varying amounts of synthesized TPABS were dissolved in DMAc at a pH ≈ 2 and mixed with the SPES solution. To obtain a sol-gel, a predetermined amount of TEOS was added to the above solution as a cross-linker and further stirred for 8 h until uniformity was achieved. The gelation process occurred by acid hydrolysis (pH ≈ 2) of silanes. The hydrogen-bonded gel matrix was cast as a film on a clean glass plate. The film was dried under ambient conditions for 24 h followed by drying at 60 °C for approximately 24 h. After drying, the membrane was peeled off, rinsed with deionised water, stored in wet conditions and cross-linked using a formal solution ($HCHO + H_2SO_4$) for 3 h at 60 °C. The prepared membranes were designated as SPES/TEOS/TPABS-*X*, where *X* is the weight percentage of TPABS to SPES (where *X* varies from 0 to 70).

2.4. Membrane characterization

FT-IR spectra of completely dried composite membranes were recorded with a Shimadzu IRPrestige-21 Fourier transform infrared (FT-IR) spectrophotometer in attenuated total reflectance (ATR) mode. The proton nuclear magnetic resonance (^{1}H NMR) spectra were collected on a Bruker ARX 600 NMR using deuterated chloroform as the solvent and tetramethylsilane ($\delta = 0$) as the internal standard.

Thermal degradation and stability of the membranes were investigated using a thermo-gravimetric analysis (TGA) (Perkin–Elmer instrument TGA 7) under a nitrogen atmosphere at a heating rate of 20 °C min^{-1} from room temperature to 600 °C. Differential scanning calorimetry (DSC) was used for thermal analysis in a temperature range of 30–300 °C. Samples of approximately 3–5 mg were loaded into aluminium pans and heated to the desired temperature at a heating rate of 5 °C min^{-1}. The oxidative stability was evaluated by immersing the membrane samples in Fenton's reagent (3% aqueous H_2O_2 + 3 ppm $FeSO_4$) at 80 °C for 1 h as reported in the literature [14].

The mechanical strength of the membrane was measured using a CMT8502 Machine model GD203A (Shenzhen Sans Testing Machine Co., Ltd, China) at a speed of 50 mm min^{-1}. Tensile tests were carried out at room temperature and ambient humidity conditions.

A cross-section of the membranes was investigated by a scanning electron microscope (SEM), using an environmental scanning electron microscope (ESEM, FEI Quanta 200) to determine the morphology of the membranes. All of the samples were soaked in liquid nitrogen and fractured, followed by sputtering with a thin layer of gold. A cross-section of the membranes was then observed using a SEM with an accelerating voltage of 30 kV. The distribution of silica and other elements in the membrane phase was recorded by energy-dispersive X-ray (EDX) measurements carried out using a HITACHI S-3000N Instrument.

To measure water uptake, the membranes were immersed in deionised water and a water–methanol mixture for 48 h, and the wet membranes were weighed after wiping the surface with tissue paper. These wet membranes were dried at a fixed temperature of 60 °C until a constant dry weight was obtained. The uptake of water was calculated using the following relationship:

$$\text{Water uptake} = \frac{W_{\text{wet}} - W_{\text{dry}}}{W_{\text{dry}}} \times 100\%, \quad (1)$$

where W_{dry}, W_{wet} are the weights of the dry and wet membranes, respectively.

The ion-exchange capacity (IEC) is defined as the ratio between the number of exchangeable ionic groups and the weight of the dry membrane. The IEC was measured by equilibrating the membrane in the 0.005 M standardised NaOH solution. The membrane was

then washed free of excess NaOH with deionised water and then, equilibrated in deionised water to remove any last traces of base. Then, the membrane was equilibrated in a 1.5 M NaCl solution for at least 72 h and the ion-exchange capacity was determined from the increase in basicity, which in turn was determined by acid–base titration with the following equation:

$$\mathrm{IEC} = \frac{V(\mathrm{NaOH}) \times C(\mathrm{NaOH})}{M(\mathrm{membrane})}, \quad (2)$$

where V (NaOH) is the volume (ml) of NaOH solution consumed, C (NaOH) is the concentration of Na^+ in the extraction solution, and M (membrane) is the dried membrane weight.

The ability of the fabricated membranes to retain water was evaluated by measuring water retention during a dynamic deswelling test. Fully swollen membranes were placed in desiccators containing silica gel at 40 °C and weighed after regular intervals. The weight of the fully swollen membranes (W_{wet}), weight of the membranes at each time step (W_t), and the weight of the dry membranes (W_{dry}) were recorded. The deswelling profile was obtained by plotting (M_t/M_0)–time curves using the following equation:

$$\frac{M_t}{M_0} = 4\left(\frac{Dt}{\Pi l^2}\right)^{1/2}, \quad (3)$$

where M_0 is the initial amount of water in the membrane ($M_0 = W_{wet} - W_{dry}$) and M_t is the amount of water remaining in the membrane at any given time ($M_t = W_t - W_{dry}$), D is the diffusion coefficient of water, and l is the membrane thickness.

The proton conductivities (δ) of the SPES/TPABS blend membranes were evaluated at different temperatures (30–80 °C) using a three-electrode electrochemical impedance spectra method with a CHI660 electrochemical workstation (CH Instruments). The sample was sandwiched between two polytetrafluoroethylene (PTFE) gaskets in a PTFE diffusion cell composed of two symmetrical chambers. The proton conductivity (δ) of the membranes was calculated from the following equation:

$$\delta = L/(RA), \quad (4)$$

where δ, L, R, and A represent the proton conductivity, membrane thickness, the resistance of the membrane and the cross-sectional area of the membrane, respectively.

An organic glass diffusion cell was used to obtain the methanol permeability of the membranes. The diffusion cell was composed of two membrane samples. One chamber of the cell (V_1) was filled with a 5 M (C_1) methanol solution in distilled water. The other chamber (V_2) was filled with water. A sample (effective area = 0.385 cm^2) was clamped between the two chambers. Methanol permeates across the membrane according to the concentration gradient between the two chambers. The methanol concentration in the receiving chamber as a function of time is given by the following equation:

$$C_2(t) = \frac{ADK\, C_1(t - t_0)}{V_2 l}, \quad (5)$$

where A (cm^2) is the membrane area, l (cm) is the membrane thickness, D is methanol diffusivity, and K is the partition coefficient between the membrane and the adjacent solution. The product DK represents membrane permeability (P):

$$P = \frac{C_2(t)V_2 l}{AC_1(t - t_0)} \quad (6)$$

C_2 is measured several times during the permeation experiment, and the methanol permeability is obtained from the slope of the straight line. The methanol concentration was measured using a gas chromatograph (Agilent GC 6820) equipped with a FID detector.

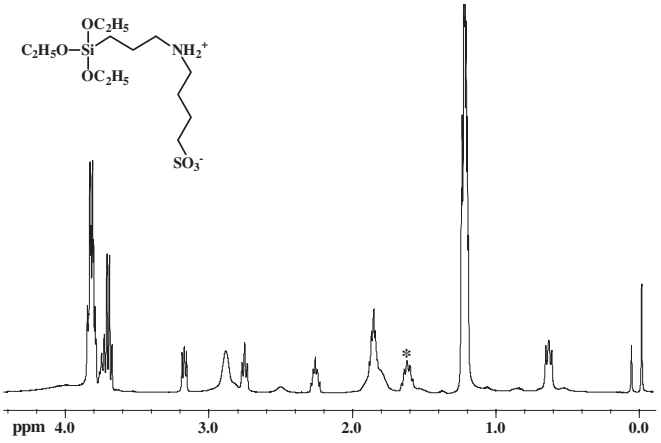

Fig. 1. ^{1}H NMR spectrum of synthesized silica precursor (TPABS).

3. Results and discussion

The degree of sulfonation of the SPES was easily controlled by changing the ratio of PES and chlorosulfonic acid [13]. TPABS was

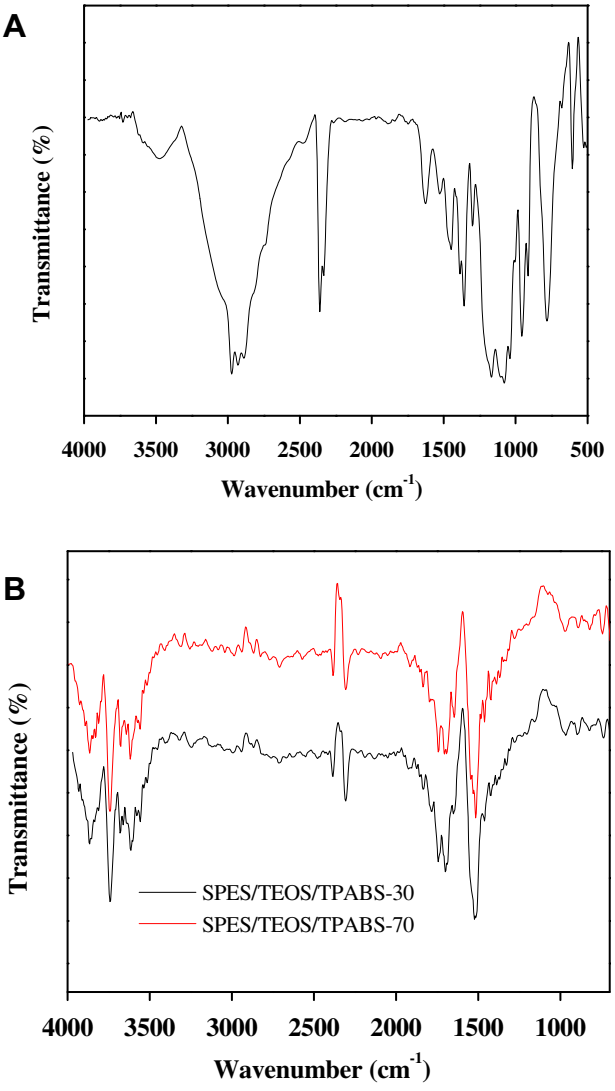

Fig. 2. FT-IR spectra of (A) TPABS and (B) the referenced cross-linked sulfonated poly(ether sulfone)s.

synthesized by the ring opening of 1,4-butane sultone with $-NH_2$ group of APTES under mild heating conditions. This was an exothermic reaction in which a proton was transferred from the amino group to 1,4-butane sultone without any side reactions [15]. The result of this reaction was the formation of an organic–inorganic silica zwitterionic precursor. ^{1}H NMR and FT-IR spectra of the desired TPABS are presented in Figs. 1 and 2A. The FT-IR spectrum for TPABS exhibited the characteristics peaks of $-SO_3H$ stretching at ~1239 cm^{-1} (asym SO_3 stretch), ~1100 cm^{-1} (sym SO_3 stretch), ~2360 to 1650 cm^{-1} (–OH stretching vibration), indicating the presence of a sulfonic acid group [16]. The strong bands near 1645 cm^{-1} and a broad absorbance in the region of 3033–2500 cm^{-1} arose due to the presence of a substituted quaternary ammonium group. In addition, there were a number of weaker bands, which are assigned as the combination peak of the Si–OR group and the amine salt group.

Generally, sol-gel processes can be carried out by acid and base catalyses. Both types of catalysed reactions (acid and base) belong to bimolecular nucleophilic substitution reactions. The acid-catalysed reaction is preceded by the rapid protonation of the –OR or –OH substituent which bonded to the silicon atom. However, in a basic environment, hydroxyl or silanolate groups firstly attack the silicon atoms forming interconnected regions of Si–O–Si bonds. These bonded regions interact cooperatively to form colloidal particles or sol. These colloidal particles further link together to yield a three-dimensional network or gel. Acid-catalysed sol-gels form linear polymers with weak cross-links ascribed to steric crowding, whereas base-catalysis yields more highly branched clusters due to rapid hydrolysis [17]. Using this knowledge, membrane-forming materials were prepared by condensation polymerization of the synthesized silica precursor (TPABS) in aqueous media by the acid-catalysed sol-gel method with SPES according to Scheme 1. The resultant gel was cast as a thin film and dried at 60 °C in a vacuum oven. The obtained water soluble thin films were cross-linked with formal solution ($HCHO + H_2SO_4$) for 3 h under thermal treatment. Organic–inorganic nanocomposites on the molecular level were achieved by designing a sol-gel method in which inorganic and organic segments were joined together through covalent or hydrogen bonds.

The ATR FT-IR spectra of the representative membranes (SPES/TEOS/TPABS-30, SPES/TEOS/TPABS-70) are given in Fig. 2B. The presence of N–H groups formed intermolecular hydrogen bonds with S=O groups on the polymer chain, which can be confirmed by observing two different peaks, one band at 3402 cm^{-1} indicating the presence of N–H asymmetric stretching, and the other at 3186 cm^{-1} ascribed to N–H symmetric stretching. The peaks in the range of 1150–1020 cm^{-1}, associated to Si–O–Si asymmetric stretching, indicate that the cross-linked network has successfully formed on the molecular level. The intensity of the peaks varied with the content of silica precursor (TPABS) in the membrane matrix. There is no doubt that presence of Si–O–Si groups is the result of the condensation reaction between hydrolysed silanol (Si–OH) groups.

The membranes with various compositions were prepared through the phase inversion method using DMAc as a solvent and deionised water as the non-solvent. SEM images of cross-sections of SPES/TEOS/TPABS-10, SPES/TEOS/TPABS-30, SPES/TEOS/TPABS-50 and SPES/TEOS/TPABS-70 membranes are shown in Fig. 3. The porous structure and distribution of silica particles can be observed in these images. The prepared hybrid membranes show a uniform and homogeneous distribution of silica particles. The pore distribution grows denser and more uniform when increasing the TPABS content from 10% to 70%, which could be attributed to the fact that the deionised water interacts with the hydrophilic TPABS through hydrogen bonding to induce a more uniform distribution of the water and pores. Furthermore, silica particles dispersed in the SPES matrix by a poly-condensation reaction exhibited a micro-phase separation. Conglomeration and aggregation in the matrix membranes were also observed, which increased with increasing silica content due to the accelerated hydrolysis of silane and its cross-linking with SPES. Elements of the membranes have been confirmed by EDX, and SPES/TEOS/TPABS-50, as a representative

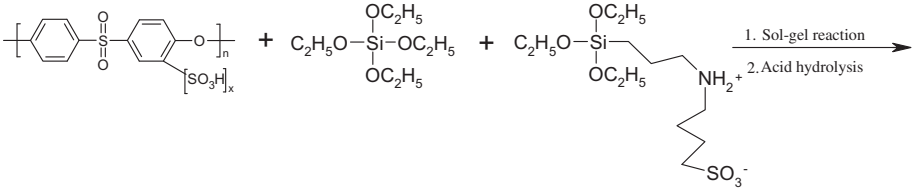

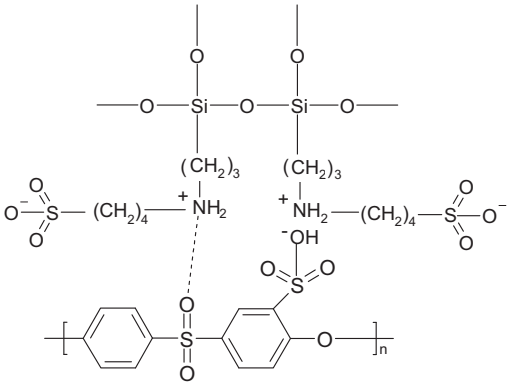

Scheme 1. Synthetic route of the hybrid membrane.

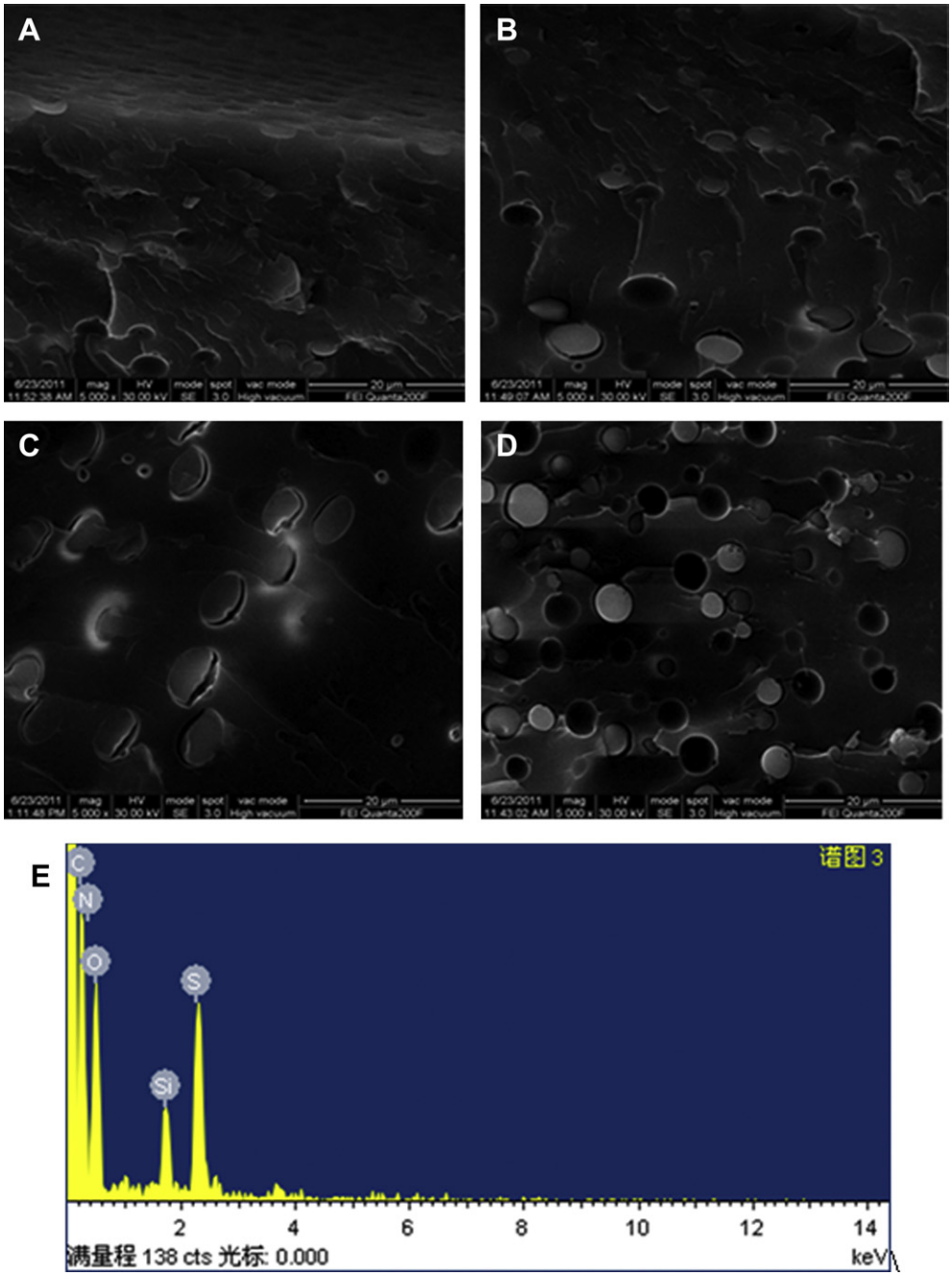

Fig. 3. SEM images of the polymer electrolyte membranes: (A) SPES/TEOS/TPABS-10; (B) SPES/TEOS/TPABS-30; (C) SPES/TEOS/TPABS-50; (D) SPES/TEOS/TPABS-70; and (E) EDX spectrum of the representative SPES/TEOS/TPABS-50 membrane.

case, clearly shows the existence of organic and inorganic constituents in the membrane matrix. The presence of Si, S and N would serve to show that TPABS was stable in the membrane matrix [18]. These results provide evidence that well-defined, cross-linked composite membranes have been successfully prepared using SPES and zwitterionic silica precursors via a sol-gel technique.

Thermo-gravimetric analysis was performed to analyse the thermal degradation stability of the nanocomposite membranes (in their H^+ form). Fig. 4 shows the TGA curves of the SPES/TEOS/TPABS-*X* referenced membranes under flowing nitrogen. In each TGA curve one can see three distinct weight-loss stages which correspond to thermal dissolution, thermal desulfonation and thermal oxidation of the polymer matrix. The first weight-loss stage between 30 and 100 °C was ascribed to the evaporation of hydrated and bound water in the membrane matrix which resulted from the condensation reaction among hydroxyl groups of silica precursor and SPES [19]. In this region, compared to uncross-linked SPES/TEOS membranes, the cross-linked membranes show a larger weight-loss, especially for SPES/TEOS/TPABS-70, most likely because of the extra bound water from the hydrophilic functional groups in the TPABS-rich membrane as well as the highly cross-linked network. The second degradation stage occurred over the temperature range of 250–300 °C, which was attributed to the loss of the sulfonic acid groups by evolution of SO_2 and SO_3 [20]. The final weight-loss (>400 °C) occurred as a decline due to the deterioration of the polymer backbone and the degradation of

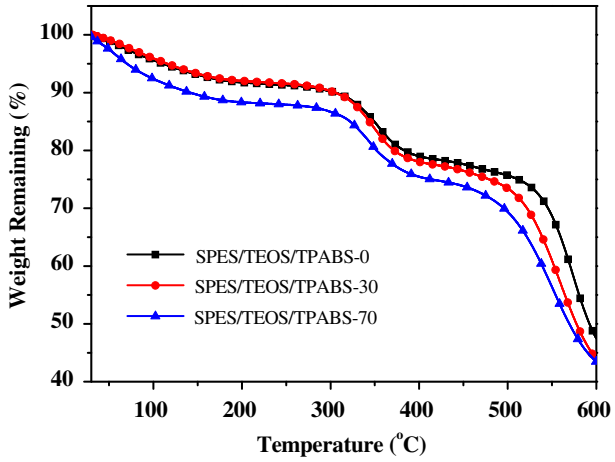

Fig. 4. TGA curves of SPES/TEOS/TPABS-*X* nanocomposite membranes.

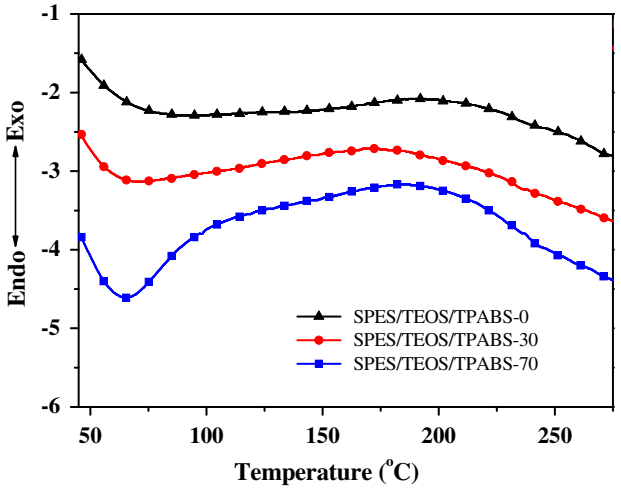

Fig. 5. DSC curves of SPES/TEOS/TPABS-*X* nanocomposite membranes.

quaternary ammonium groups [21]. The good stability supports that these organic–inorganic nanocomposites are suitable for DMFC application.

Fig. 5 depicts DSC thermograms of representative hybrid SPES/TEOS/TPABS membranes with different silica content to evaluate the glass transition temperature (T_g) and thermal stability of the membranes. The incorporation of a silica precursor (TPABS) into the SPES matrix had a profound effect on their T_g values. The endothermic peaks in accordance with the T_g values were found to be at approximately 79.68 °C, 70.42 °C, and 64.85 °C, respectively. The T_g values decreased with an increase in TPABS content, which can be interpreted as an enhanced degree of cross-linking deteriorating the crystalline nature of the SPES matrix.

Table 2
The mechanical properties for different membranes.

Membrane	Tensile strength (MPa)	Elongation at break (%)	Elastic modulus (GPa)
SPES/TEOS/TPABS-0	39.43	9.15	0.67
SPES/TEOS/TPABS-10	42.67	8.67	0.72
SPES/TEOS/TPABS-30	48.56	8.23	0.89
SPES/TEOS/TPABS-50	50.01	7.97	0.94
SPES/TEOS/TPABS-70	51.32	7.30	1.13
Nafion® 117	26.1	194	0.24

Membrane stability and durability are crucial factors used to evaluate the feasibility and possibility of DMFCs under operating conditions. The formation of H_2O_2, •OH and •OOH radicals during water decomposition was believed to attack hydrogen-containing bonds in proton exchange membranes. Weight-loss of the prepared membranes was tested in Fenton's reagent (3 ppm $FeSO_4$ + 3% H_2O_2) for 1 h at 80 °C and the results are revealed as oxidative weight-loss percentages (W_{OX}) in Table 1. Free peroxy radical attacks are more aggressive at high temperatures and occur in proximity to hydrophilic domains [22]. Generally, silica blocks the hydrogen-containing hydrophilic pores because it forms cross-linked structure. The lifetime of •OH and •OOH radicals is extremely short [23], which makes penetrating inside siloxane-containing domains difficult. Therefore, the excellent oxidative stability of these membranes can be attributed to these cross-linked structures. However, from Table 1, we can see that weight-loss increased with increasing content of TPABS in the membranes and that SPES/TEOS/TPABS-70 exhibited the greatest weight-loss, most likely owing to its high degree of hydrophilic functionality and hydrogen-containing groups.

Table 2 lists the mechanical properties of the SPES/TEOS/TPABS membranes as evaluated at room temperature and ambient humility. The composite membranes possessed high tensile strength and elastic modulus values in the ranges of 39.43–51.32 MPa and 0.67–1.13 GPa, respectively, which are higher than those of Nafion® 117. The elongation at break of all membranes ranged from 9.15 to 7.30%. The tensile strength of the nanocomposite membranes all obviously increased with an increase of silica content. Similar trends can be observed for elastic modulus as well, while elongation at break showed the contrary tendency. It is because the formation of a dimensional network of Si–O–Si groups and hydrophilic ionic channels increased the interactions between molecular chains, restricting the stretching of the polymer backbone and hindering the strain with extension. Meanwhile, the polymer chains became stiffer and more brittle due to the Si–O–Si structure. However, from mechanical testing, it can be concluded that the mechanical properties of the composite membranes is good enough to meet the requirements of DMFC applications.

Water uptake is an important factor that directly determines whether membranes will have good properties, such as proton conductivity, mechanical and dimensional stability [24]. The water within the membrane provides a carrier for the protons and helps

Table 1
Water uptake (λ_W), water–methanol uptake (λ_{W+MeOH}), ion-exchange capacity (IEC), proton conductivity (δ), methanol permeability (P), activation energy (E_a), and selectivity parameter (SP) values, oxidative weight-loss (W_{OX}), and water diffusion coefficient (D) values for different membranes.

membrane	λ_W (wt %)	λ_{W+MeOH} (wt %)	IEC (mequiv g^{-1})	δ (10^{-2} S cm^{-1})	P (10^{-7} cm^2 s^{-1})	E_a (KJ mol^{-1})	SP (10^5 S cm^{-3} s)	W_{OX} (wt %)	D (10^{-6} cm^2 s)
SPES/TEOS/TPABS-0	21.43	19.26	0.85	1.14	0.66	11.27	1.67	4.37	1.09
SPES/TEOS/TPABS-10	25.04	23.50	1.02	1.81	0.78	10.11	1.54	5.26	1.10
SPES/TEOS/TPABS-30	34.34	30.29	1.06	3.89	1.36	8.19	2.03	7.95	1.11
SPES/TEOS/TPABS-50	41.89	38.45	1.11	5.13	1.64	7.49	2.47	9.78	1.11
SPES/TEOS/TPABS-70	43.38	42.88	1.37	7.24	2.46	6.63	2.63	10.35	1.12

to maintain high proton conductivity. Excessive volume fraction of water in the membrane phase, however, can reduce dimensional and thermal stabilities as well as proton concentration. The dissociation of functional groups is responsible for the presence of water in the membrane matrix. Table 1 shows solvent uptake values (λ_W and λ_{W+MeOH}, measured in water and water–methanol mixtures, respectively) for different membranes. The solvent uptake characteristics of the membranes increased with increasing TPABS silica content, perhaps because more functional hydrophilic groups were available for hydrogen bonding with water. It is worthy to note that the λ_{W+MeOH} values are lower than the λ_W values, suggesting that the moderate water/methanol solvent uptakes could maintain good dimensional stability of the cross-linked membranes in practical application.

Water vapour sorption and diffusion properties in PEMs are crucial for DMFCs' applicability and have significant effects on proton conductivity. The water retention capability ($(M_t/M_0) - t$ (time) curves) of cross-linked membranes was illustrated in Fig. 6. The water retention capability dramatically improved with the degree of cross-linking and the increasing amount of TPABS. Water desorption kinetics of the developed membranes was further evaluated by plotting ($M_t/M_0 - t^{1/2}$) curves as a function of time in Fig. 6 using Eq.(7) and then calculating the water diffusion coefficient (D) derived from Higuchi's model [25].

$$\frac{M_t}{M_0} = -kt^{1/2} + 1 \quad (7)$$

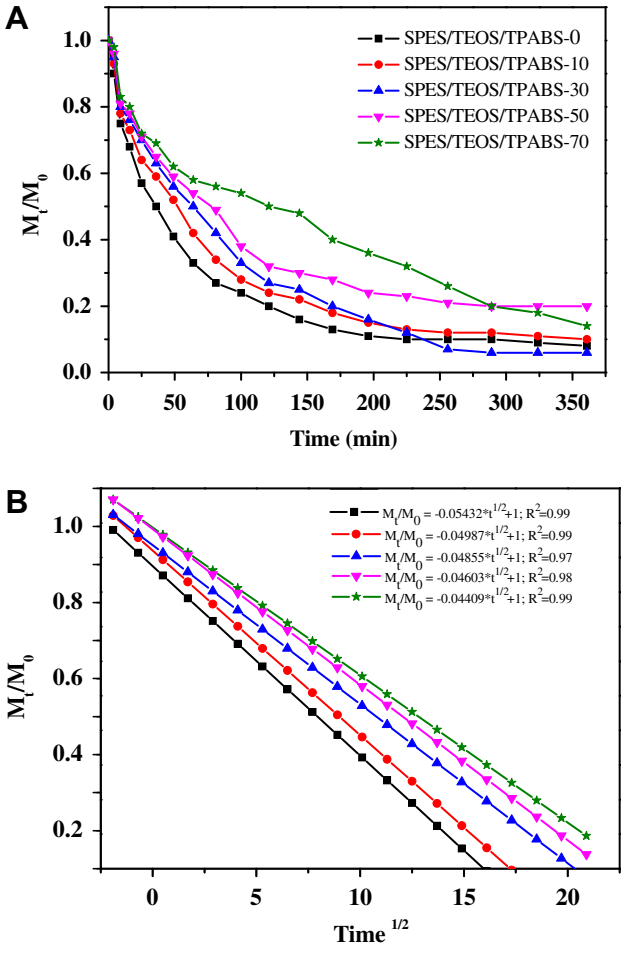

Fig. 6. Water desorption profile for SPES/TEOS/TPABS-*X* membranes: (A) isotherm at 40 °C; (B) Higuchi's model fit of the deswelling behaviour.

where M_0 and M_t are the initial amount of water and the water remaining in the polymer matrix at any given time, respectively, and k is a constant.

Straight lines based on variation of silica precursor (TPABS) content fit Higuchi's model, and indicated a diffusion-controlled water desorption mechanism. The rate of water desorption decreased with an increase of the TPABS content. TPABS acted as a binder for water in the SPES/TEOS/TPABS-*X* matrix due to the formation of hydrophilic ionic channels and siloxane cages. On the other hand, the cross-linked structure further fixed the water in the network. The diffusion coefficient of water was investigated using a best-fit normalised mass change method and is shown in Table 1. Water diffusion coefficient values (D) showed a similar trend to the water retention capability of various membranes. Therefore, both the TPABS silica and cross-linking density acted as a barrier which hindered the release of water and enhanced the water retention capacity of the fabricated membranes even at higher temperatures.

The ion-exchange capacity (IEC) indicates the density of ionisable hydrophilic functional groups, which has a direct influence on water uptake and proton transportation. All of the membranes exhibited excellent IEC values, which ranged from 0.85 to 1.37 mequiv g^{-1} and increased with an increase of the TPABS content in matrix membrane (Table 1). SPES/TEOS/TPABS-70 had the highest IEC value of 1.37 mequiv g^{-1}, while Nafion® 117 showed a lower (0.90 mequiv g^{-1}) value [7]. The IEC rose due to the presence of sulfonated acid groups and quaternary ammonium groups in the system.

The proton conductivity of organic–inorganic hybrid PEMs is a key property that affects fuel cell performance. This value was measured from 30 °C to 80 °C under 100% RH (relative humility) for hydrated membranes, and relevant data for 30 °C are presented in Table 1. It was noteworthy that the proton conductivity was improved with an increase in the TPABS content. The SPES/TEOS/TPABS-70 membrane showed the highest proton conductivity at 7.24×10^{-2} S cm^{-1}, on the same order of magnitude as Nafion® 117 (9.56×10^{-2} S cm^{-1}) [7]. This promising result may be due to two reasons: (i) the more sulfonic acid groups facilitated proton transport and (ii) the moderate water retention ability resulting from the cross-linked structure and the hydrophilic silica moieties forms beneficial proton-conduction pathways.

The temperature dependence of proton conductivity of the fabricated membranes is shown in Fig. 7. Fortunately, in contrast with pristine SPES/TEOS/TPABS-0, by introducing the TPABS into the polymer matrix, proton conductivity increased linearly with the increase in temperature. Elevated temperatures favour the dynamics of proton transport and the excellent water retention

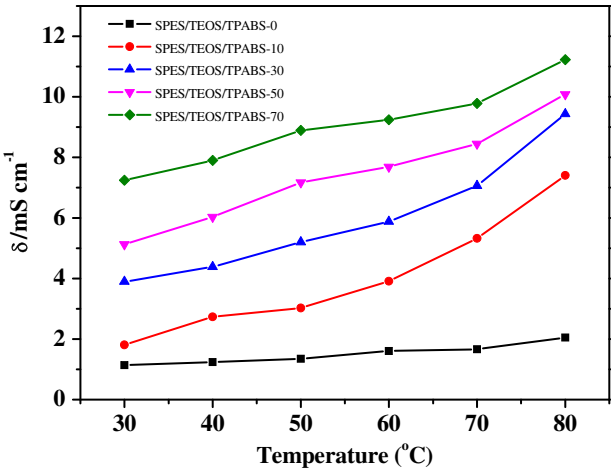

Fig. 7. Proton conductivity of the prepared membranes at different temperatures.

ability maintains the increased proton conductivity at high temperatures.

Membrane proton conductivity data obtained at elevated temperatures (from 30 °C to 80 °C) under 100% relative humidity are presented in Fig. 8 as an Arrhenius plot for the estimation of the activation energy (E_a), the minimum energy required for proton transportation across the membrane. Assuming that the conductivity follows Arrhenius behaviour, the proton transport activation energy of the nanocomposite membrane can be obtained by the following equation [26]:

$$E_a = -b \times R, \quad (8)$$

where b is the slope of the regression line of $\ln \delta$ (S cm^{-1}) vs. 1000/T (K^{-1}) and R is the gas constant (8.314 J K^{-1} mol^{-1}). The E_a values decreased from 11.27 to 6.63 kJ mol^{-1} when the TPABS content increased in the membrane matrix. For the fabricated membranes, the E_a values were only slightly higher in comparison with a Nafion®117 membrane (6.52 kJ mol^{-1}) [18]; therefore, the membranes reveal a positive temperature–conductivity dependency.

The methanol permeability profiles for all SPES/TEOS/TPABS membranes were determined using Eq. (6), and the relevant data obtained are presented in Table 1. Methanol permeability coefficients for these SPES/TEOS/TPABS membranes ($0.66–2.47 \times 10^{-7}$ cm^2 s^{-1}) were one order of magnitude lower in comparison with Nafion®117 (1.310×10^{-6} cm^2 s^{-1}) [12]. The permeation of liquid molecules across the polymer membrane happened via a diffusion mechanism, and the permeability of the penetrate (methanol in this case) is the product of its solubility and diffusivity [27]. The cross-linked structures hindered methanol penetration through the membrane due to the narrow free-void volume. Methanol permeability also increased with increasing TPABS content due to the pronounced hydrophilicity of TPABS.

$$SP = \frac{\delta}{P_{MeOH}} \quad (9)$$

To directly compare the applicability of nanocomposite SPES/TEOS/TPABS for DMFC applications, the ratio of proton conductivity and methanol permeability (δ/P) data were measured as a selectivity parameter (SP) using Eq. (9) and are presented in Fig. 9. SPES/TEOS/TPABS-70 exhibited an SP value of 2.63×10^5 S cm^{-3} s, while the SP for Nafion®117 was 0.72×10^5 S cm^{-3} s at 30 °C [6]. This observation was ascribed to the relatively low methanol permeability and high proton conductivity of the developed membranes.

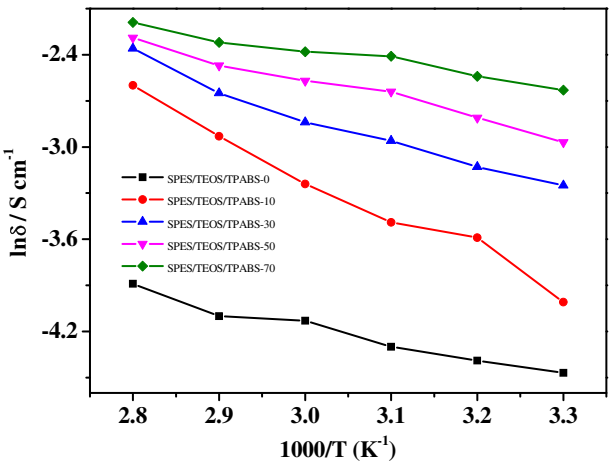

Fig. 8. Arrhenius plot under 100% RH environment for different nanocomposite membranes.

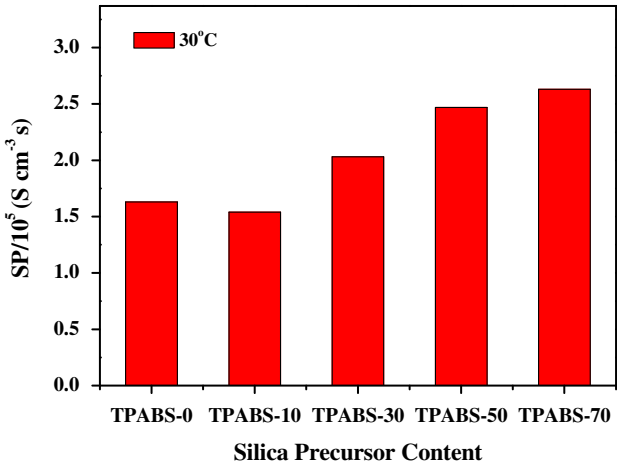

Fig. 9. Selectivity parameter values for different membranes at 30 °C temperature.

The SP values slightly decreased at first and then increased with an increase of silica content, and reached a maximum at 2.63 S cm^{-3} s when the TPABS content was 70% wt. to SPES in the membrane matrix. Thus, a better understanding of polymer structure and membrane performance, in terms of permeability and selectivity, enables us to tailor the membrane structure for specific purposes.

4. Conclusions

We reported a simple and feasible procedure for the production of nanocomposite, hybrid-cross-linked membranes synthesized with SPES and zwitterionic silica though an acid-catalysed sol-gel process in aqueous conditions. By the incorporation of the zwitterionic molecules, the silica particles were homogenously dispersed into the SPES matrix, which leaded to well-defined cross-linked structures. The thermal stabilities (thermally stable up to 200°C in a dry nitrogen atmosphere) of the membranes were also improved with the incorporation of TPABS. Although the elongation at break of all membranes decreased with increasing silica content (ranged from 9.15 to 7.30%), the cross-linked networks endowed the composite membranes with high tensile strength and elastic moduli in the ranges of 39.43–51.32 MPa, 0.67–1.13 GPa, respectively, which are higher than those of Nafion® 117. The highly concentrated sulfonic acid groups and cross-linked structures also created a good balance between proton conductivity and low fuel permeability. These membranes possessed high proton conductivities, up to 7.24×10^{-2} S cm^{-1}, whereas their methanol permeability has been dramatically reduced to $0.66–2.47 \times 10^{-7}$ cm^2 s^{-1}, making these membranes good potential polymer electrolyte membranes for DMFCs' application. Therefore, the development of cross-linked zwitterionic polyelectrolyte membranes via sol-gel processes provides an effective and simple route for the preparation of proton exchange membranes with good proton conductivity and low fuel permeability.

Acknowledgements

Financial support for this work was provided by the National Natural Science Foundation of China (21164007).

References

[1] T.J. Peckham, S. Holdcroft, Adv. Mater. 22 (2010) 4667–4690.
[2] C. Zhou, M.A. Guerra, Z.-M. Qiu, T.A. Zawodzinski, D.A. Schiraldi, Macromolecules 40 (2007) 8695–8707.

[3] J. Xie, F. Xu, D.L. Wood Iii, K.L. More, T.A. Zawodzinski, W.H. Smith, Electrochim. Acta 55 (2010) 7404–7412.
[4] H. Zhang, Z. Zhou, Polym. Adv. Technol. 19 (2008) 425–431.
[5] H. Luo, G. Vaivars, M. Mathe, J. Power Sources 195 (2010) 5197–5200; P.P. Chu, C.-S. Wu, P.-C. Liu, T.-H. Wang, J.-P. Pan, Polymer 51 (2010) 1386–1394; Y.-S. Ye, Y.-C. Yen, C.-C. Cheng, W.-Y. Chen, L.-T. Tsai, F.-C. Chang, Polymer 50 (2009) 3196–3203.
[6] B.P. Tripathi, V.K. Shahi, J. Phys. Chem. B 112 (2008) 15678–15690.
[7] B.P. Tripathi, M. Kumar, V.K. Shahi, J. Membr. Sci. 360 (2010) 90–101.
[8] B.P. Tripathi, T. Chakrabarty, V.K. Shahi, J. Mater. Chem. 20 (2010) 8036–8044.
[9] S.J. Peighambardoust, S. Rowshanzamir, M. Amjadi, Int. J. Hydrogen Energy 35 (2010) 9349–9384.
[10] Y. Patil, K.A. Mauritz, J. Appl. Polym. Sci. 113 (2009) 3269–3278.
[11] F. Pereira, K. Vallé, P. Belleville, A. Morin, S. Lambert, C. Sanchez, Chem. Mater. 20 (2008) 1710–1718.
[12] B.P. Tripathi, V.K. Shahi, ACS Appl. Mater. Interfaces 1 (2009) 1002–1012.
[13] H. Dai, R. Guan, C. Li, J. Liu, Solid State Ionics 178 (2007) 339–345.
[14] B.P. Tripathi, A. Saxena, V.K. Shahi, J. Membr. Sci. 318 (2008) 288–297.
[15] R.F. Fischer, Ind. Eng. Chem. 56 (1964) 41–45.
[16] G. Socrates, Infrared Characteristic Group Frequencies, Wiley, New York, 1980.
[17] R.K. Nagarale, G.S. Gohil, V.K. Shahi, R. Rangarajan, Macromolecules 37 (2004) 10023–10030;
C.J. Brinker, D.E. Clark, D.R. Ulrich, Better ceramics through chemistry III. In: Proceedings of the Symposium, Reno, NV; Apr. 5–9, 1988.
[18] R. Guan, H. Zou, D. Lu, C. Gong, Y. Liu, Eur. Polym. J. 41 (2005) 1554–1560.
[19] J. Qiao, T. Hamaya, T. Okada, J. Mater. Chem. 15 (2005) 4414–4423.
[20] H. Li, Z. Cui, C. Zhao, J. Wu, T. Fu, Y. Zhang, K. Shao, H. Zhang, H. Na, W. Xing, J. Membr. Sci. 343 (2009) 164–170.
[21] Y. Xiong, Q.L. Liu, Q.G. Zhang, A.M. Zhu, J. Power Sources 183 (2008) 447–453.
[22] N. Asano, M. Aoki, S. Suzuki, K. Miyatake, H. Uchida, M. Watanabe, J. Am. Chem. Soc. 128 (2006) 1762–1769.
[23] T. Yamaguchi, H. Zhou, S. Nakazawa, N. Hara, Adv. Mater. 19 (2007) 592–596.
[24] D.B. Spry, A. Goun, K. Glusac, D.E. Moilanen, M.D. Fayer, J. Am. Chem. Soc. 129 (2007) 8122–8130.
[25] T.-Y. Liu, S.-Y. Chen, Y.-L. Lin, D.-M. Liu, Langmuir 22 (2006) 9740–9745.
[26] M.K. Ravikumar, A.K. Shukla, J. Electrochem. Soc. 143 (1996) 2601–2606.
[27] B.P. Ladewig, R.B. Knott, A.J. Hill, J.D. Riches, J.W. White, D.J. Martin, J.C. Diniz da Costa, G.Q. Lu, Chem. Mater. 19 (2007) 2372–2381.